Toward Understanding the Electron Density Distribution in Magnetic Clusters: Insight from the ELF and AIM Analyses of Ground-State Fe_4

Slawomir Berski*

Faculty of Chemistry, University of Wroclaw, F. Joliot-Curie 14, 50-383 Wroclaw, Poland, and Departament de Ciències Experimentals, Universitat Jaume I, Apartat 224, 12080, Castelló, Spain

Gennady L. Gutsev* and Mogus D. Mochena

Department of Physics, Florida A&M University, Tallahassee, Florida 32307

Juan Andrés

Departament de Ciències Experimentals, Universitat Jaume I, Apartat 224, 12080, Castelló, Spain

Received: March 18, 2004; In Final Form: May 3, 2004

Topological analysis of the electron localization function (ELF) in the ground-state Fe_4 cluster reveals different regions of valence electron localization in terms of monosynaptic V(Fe_i), disynaptic V(Fe_i,Fe_j), trisynaptic V(Fe_i,Fe_j,Fe_k), and tetrasynaptic V(Fe_1,Fe_2,Fe_3,Fe_4) bonding valence attractors and basins. The degree of electron localization is found to be smaller than in a homogeneous electron gas with $\eta(\mathbf{r}) \leq 0.490$. A relative fluctuation of the electron density in the valence basins ranges between 0.83 and 0.96, which indicates a rather substantial delocalization of the electron density. Approximately three valence α-electrons are localized at each iron core C($Fe_{i=1,4}$) while two α-electrons, i.e., 0.5 e per one atom, are delocalized over the cluster. The valence electrons show a trend toward localization between iron sites and in the proximity of triangular faces of the cluster with the basin population of one electron. Metallic bonds in Fe_4 may be characterized as partially covalent and highly delocalized both spatially and electronically, which is reflected by a large number of local maxima and relatively large fluctuations, respectively.

1. Introduction

Iron clusters have been the subject of numerous experimental[1] and theoretical[2,3] studies. The results of computations[4] performed using density function theory with the generalized gradient approximation (DFT-GGA) for the exchange-correlation potential appear to be rather reliable. The most recent study[5] of Fe_n, Fe_n^-, and Fe_n^+ ($n = 2-6$) have shown the DFT-GGA results to be in rather good agreement with experimentally obtained electron affinities, ionization energies, and thermodynamic data.

Yet, the understanding of chemical bonding in iron clusters is apparently lacking. Traditional methods such as natural bond analysis (NBO)[6] met difficulties in describing the chemical bonding in complexes containing a single 3d-metal atom.[7] Iron clusters are anticipated to possess a strong 4s−3d hybridization and, therefore, to be intractable for the NBO analysis. Thus, one needs to resort to a method that does not rely on a localization scheme in terms of transformations of molecular orbitals composed of atomic orbitals (a traditional MO-LCAO scheme). The latter is justifiable if the classic bond description is valid, e.g., in 3d-metal dimers.[8]

A promising approach for analyzing the chemical bonding was introduced by Becke and Edgecombe[9] and presents a topological analysis of the electron localization function. This analysis is based on the previous suggestion of Bader et al.[10] to use the Laplacian of the electronic density for characterizing atomic interactions. We choose Fe_4 as a representative of magnetic materials, since this tetramer possesses a three-dimensional nuclear frame.

* Corresponding authors: berski@nuvol.uji.es; gennady.gutsev@famu.edu.

The paper is organized as follows. First we describe the principles of topological analysis of scalar fields and properties of the electron localization function. Next, brief details of computations are presented followed by the discussion of the results obtained. The last section summarizes our findings.

2. Methods of Topological Analysis

Topological analysis of the electron localization function (ELF)[9,11−12] presents a mathematical model of Lewis's valence theory[13,14] and provides a partition of the molecular space into basins of attractors that are in a one-to-one correspondence with expected chemical properties. Several interpretations of the ELF chemical meaning have been proposed.[9,15−19] Originally, this function was designed by Becke and Edgecombe[9] in order to provide an orbital-independent description of electron localization. Their expression for the ELF is

$$\eta(\mathbf{r}) = \frac{1}{1 + \left(\frac{D_\sigma}{D_\sigma^0}\right)^2} \tag{1}$$

where D_σ and D_σ^0 represent the curvature of the electron pair density of the same spin σ for a real system (the Fermi hole curvature) and the homogeneous electron gas of the same density, respectively. By definition, the ELF values are confined between 0 and 1. The original derivation was based on the Laplacian of conditional Hartree−Fock probability of finding a σ-spin electron at $\mathbf{r}_2$ when another σ-spin electron is located at $\mathbf{r}_1$, namely:

$$D_\sigma = (\nabla_2^2 P_{\mathrm{cond}}^{\sigma\sigma}(1,2))_{1=2} = \sum_{i=1}^{i=N} |\nabla\varphi_i|^2 - \frac{1}{4}\frac{|\nabla\rho^\sigma(1)|^2}{\rho^\sigma(1)} \tag{2}$$

10.1021/jp0487814 CCC: $27.50
Published on Web 06/17/2004

is expressed in terms of orbital contributions. $D_\sigma^0(\mathbf{r})$ is the Thomas-Fermi kinetic energy for the homogeneous electron gas of the same electronic density:

$$D_\sigma^0(\mathbf{r}) = C_F \rho(\mathbf{r})^{5/3} \tag{3}$$

where C_F is the Fermi constant. In regions dominated by the antiparallel spin coupling, the ELF is close to 1. In the vicinity of boundaries between two such regions, electrons of the same spin may approach closer to each other, and the ELF has smaller values.

Savin et al.[15] expressed the ELF in terms of the local kinetic energy density, which increases due to the Pauli repulsion $T_S(\mathbf{r}) - T_{vW}(\mathbf{r})$:

$$\eta(\mathbf{r}) = \left[1 + \left(\frac{T_S(\mathbf{r}) - T_{vW}(\mathbf{r})}{T_{TF}(\mathbf{r})}\right)^2\right]^{-1} \tag{4}$$

where $T_S(\mathbf{r})$ is the local positive kinetic energy of a system of noninteracting fermions having the same density as the real system, $T_{vW}(\mathbf{r})$ is the von Weizsäcker kinetic energy functional, and $T_{TF}(\mathbf{r})$ is the local kinetic energy of a homogeneous electron gas. The $T_S(\mathbf{r}) - T_{vW}(\mathbf{r})$ term corresponds to an excessive local kinetic energy due to the Pauli repulsion. Dobson[16,17] proposed two different interpretations for the Fermi hole curvature D_σ that provides a useful measure of both the number of the same spin electrons in the vicinity of an electron at $\mathbf{r}$ and the density of relative kinetic energy of electron pairs of the same spin σ near $\mathbf{r}$.

Burdett and McCormick[18] proposed an interpretation that relates the ELF and the nodal properties of the occupied orbitals. High values of the ELF correspond to points where the electron density is high, but only few or no nodes pass through the points. On the contrary, the ELF values are small in points where the electron density is low or if there are enough nodes to overcome contributions from the electron density. Kohout[19] emphasized the lacking direct relationship between small values of the ELF calculated for regions with low electron densities. He also noticed that regions of large ELF values might be formed outside the core regions in compounds where inner-shell electrons may participate in the bonding.

Recently, Silvi[20] described the electronic cloud in terms of a "chemical electron gas" characterized by scalar fields of the electron density and the spin-pair composition c_π, which is defined by

$$c_\pi(\mathbf{r}) = q^{-2/3} \frac{\bar{N}_V^{\alpha\alpha}(\mathbf{r}) + \bar{N}_V^{\beta\beta}(\mathbf{r})}{2\bar{N}_V^{\alpha\beta}(\mathbf{r})} \tag{5}$$

where $\bar{N}_V^{\alpha\alpha}(\mathbf{r})$, $\bar{N}_V^{\beta\beta}(\mathbf{r})$, and $\bar{N}_V^{\alpha\beta}(\mathbf{r})$ are the pair functions integrated over the volume V centered at the reference point with population q. Actually, $c_\pi(\mathbf{r})$ is the concentration ratio of parallel and antiparallel spin pairs at a given point. For a closed-shell single determinant wave function, $c_\pi(\mathbf{r})$ can be approximated within a constant by the D_σ/D_σ^0 ratio used in eq 1 in the definition of the electron localization function $\eta(\mathbf{r})$.

The $\eta(\mathbf{r})$ function depends on a set of parameters $\{\alpha\}$, such as nuclear coordinates, electronic state of the system, etc., and is characterized by critical points $\mathbf{r}_C$ where

$$\nabla\eta(\mathbf{r}_C;\{\alpha\}) = 0 \tag{6}$$

The number of positive eigenvalues of the Hessian matrix of $\eta(\mathbf{r})$ at a particular $\mathbf{r}_C$ is referred to as the index $I(P)$, which ranges from 0 to 3 in $\mathbf{R}^3$. The local maxima of $\eta(\mathbf{r})$ are critical points with $I(P) = 0$. If a critical point corresponds to a maximum, then it acts as an attractor to a multitude of gradient paths that form a basin. Separatrices, represented by bounding surfaces, lines, or single points that separate the basins, are stable manifolds of critical points possessing at least one strictly positive index. There are typically two kinds of basins: core basins C(A) encompassing nuclei A with $Z > 2$ and valence basins V(A,B). The synaptic order of a valence basin is defined[21,22] as the number of core basins with which the valence basin shares common boundaries. A valence basin encompassing a proton is considered as a formal core basin. Monosynaptic, disynaptic, and polysynaptic basins are associated with lone pairs, two-center bonds, and multicenter bonds, respectively. The population of a basin is obtained by integrating the electron density over the basin volume Ω_i:

$$\bar{N}(\Omega_i) = \int_{\Omega_i} \rho(\mathbf{r})\, d\mathbf{r} = \bar{N}^\alpha(\Omega_i) + \bar{N}^\beta(\Omega_i) \tag{7}$$

A useful quantity is the variance of a basin population defined as

$$\sigma^2(\bar{N};\Omega_i) = \int_{\Omega_i} d\mathbf{r}_1 \int_{\Omega_i} \pi(\mathbf{r}_1,\mathbf{r}_2)\, d\mathbf{r}_2 - [\bar{N}(\Omega_i)]^2 + \bar{N}(\Omega_i) \tag{8}$$

where $\pi(\mathbf{r}_1,\mathbf{r}_2)$ is the spin-independent pair function. The variance is a measure of quantum mechanical uncertainty of a basin population and can be rewritten in terms of contributions from other basins as

$$\sigma^2(\bar{N};\Omega_i) = \sum_{j\neq i} \bar{N}(\Omega_i)\bar{N}(\Omega_j) - \bar{N}(\Omega_i,\Omega_j) = \sum_{j\neq i} \mathrm{cov}(\Omega_i,\Omega_j) \tag{9}$$

where the product $\bar{N}(\Omega_i)\bar{N}(\Omega_j)$ represents the number of electron pairs classically expected from the basin populations, and $\bar{N}(\Omega_i,\Omega_j)$ is the actual number of pairs obtained by integration of the pair function over the basins Ω_i and Ω_j. The pair covariance function $\mathrm{cov}(\Omega_i,\Omega_j)$ indicates the extent in which population fluctuations of two basins are correlated. Following Bader and Stevens[23] who introduced the concept of fluctuation $\Lambda(\bar{N},\Omega)$ around the basin population over the region Ω, one may define a relative fluctuation of the Ω_i basin population as

$$\lambda(\bar{N};\Omega_i) = \frac{\sigma^2(\bar{N},\Omega_i)}{\bar{N}(\Omega_i)} \tag{10}$$

It is positive and is expected to be smaller than 1.0 in majority of cases.

3. Computational Details

The electronic density used for the ELF analysis was obtained from optimizations of the ground state of Fe_4, which has[4,5] fourteen unpaired electrons. The standard approach where linear combinations of atomic orbitals centered at iron sites constitute Kohn−Sham [24] one-electron orbitals was used. Optimizations are performed using the Gaussian 98 program [25] and the 6-311+G* (15s11p6d1f)/[10s7p4d1f] basis set.[26−28] The exchange-correlation functional presents a combination of the gradient corrected exchange due to Becke[29] and correlation due to Perdew and Wang.[30] No symmetry constraint was imposed and optimizations arrived at an actual D_{2d} configuration: $R_{1,2} = R_{3,4} = 2.55$ Å, all other $R_{ij} = 2.26$ Å. The local magnetic moments derived from the conventional Mulliken analysis yields values of 3.5 μ_B at each atom site.

TABLE 1: Topological Data Calculated for the Fe_4 Cluster

no	attractor/basin Ω_i[a]	η	R [Å]	$\bar{N}$[e]	$\langle S_z \rangle$[e]	$\sigma^2(\bar{N})$	$\lambda = \sigma^2/\bar{N}$
1	$C(Fe_{i=1,4})$	1.000		23.78	1.47	1.92	0.08
2	$V(Fe_{i=1,4})$	0.279	1.979	0.26	0.09	0.24	0.92
3	$V_1(Fe_1,Fe_3)$	0.490	1.971 (both Fe_1 and Fe_3)	0.66	0.15	0.57	0.87
4	$V_2(Fe_1,F_3)$	0.438	1.424 (both Fe_1 and Fe_3)	0.33	0.01	0.30	0.91
5	$V(Fe_1,Fe_2,Fe_3)$	0.469	1.803 (Fe_1 and Fe_2), 1.825(Fe_3)	0.94	0.03	0.78	0.83
6	$V(Fe_1,Fe_2,Fe_3,Fe_4)$	0.341	1.450 (for each Fe)	0.14	0.00	0.13	0.96

[a] Some exemplary attractors/basins are chosen. η is the value of a local maximum found in the ELF gradient field. R is the distance between a given attractor and Fe nucleus. $\bar{N}$ is the mean electron population of the Ω_i basin, $\bar{N}(\Omega_i) = \bar{N}(\Omega) + \bar{N}^\beta(\Omega_i)$. $\langle S_z \rangle$ is the integrated spin density defined as $S_Z(\Omega_i) = 1/2 \int_{\Omega_i} (\rho^\alpha(\mathbf{r}) - \rho^\beta(\mathbf{r}))\, d\mathbf{r}$. $\sigma^2(\bar{N})$ is the variance of the basin population. $\lambda = \sigma^2/\bar{N}$ is the relative fluctuation.

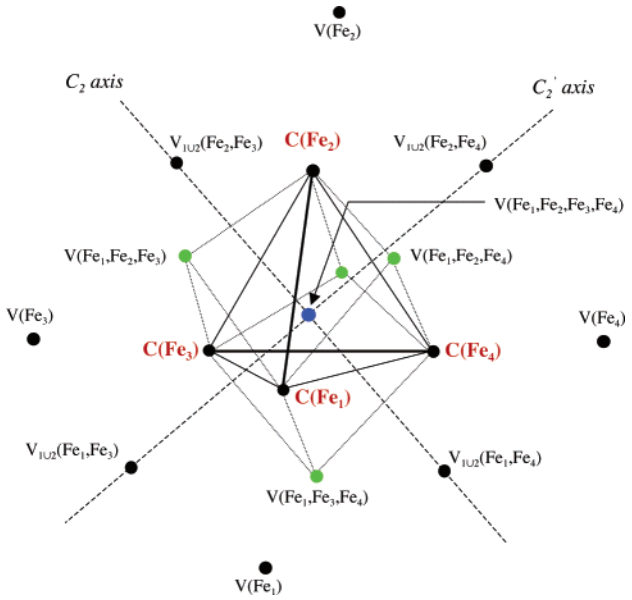

Figure 1. Three-dimensional representation of the Fe_4 cluster attractors. The longer Fe_1-Fe_2 and Fe_3-Fe_4 distances are shown by the thin lines. The dotted lines connecting the valence trisynaptic $V(Fe_i,Fe_j,Fe_k)$ attractors with the core attractors $C(Fe_i)$ reflect the "synaptic order" of localization basins associated with them. For the disynaptic attractors $V(Fe_{i=1,2},Fe_{j=3,4})$, only the $V_1(Fe_{i=1,2},Fe_{j=3,4})$ attractors are shown, see text.

A topological analysis of the electron localization function was performed using the TopMod software,[31,32] and the ELF function was visualized using the SciAn program.[32] The electron density integrations over localization basins were carried out using a rectangular parallelepiped grid ($200 \times 200 \times 185$) with a step of 0.07 Bohr. Critical points of the electron density gradient field were localized using the module Extreme from the AIMPAC suit.[34]

4. Results and Discussion

An analysis of the ELF gradient field of Fe_4 reveals twenty-one attractors (local maxima), four of which are associated with the core electron densities. The attractors are presented in Figure 1 while the ELF (η) values and distances (R) from the atomic nuclei are given in Table 1. The electron densities of core regions are characterized by point attractors $C(Fe_{i=1,4})$ whose positions coincide with the positions of the Fe nuclei.

It is rather common to consider the electronic shell structure in metal clusters as corresponding to a free-electron-like distribution which yields $\eta = 0.5$.[35] However, all the valence attractors of Fe_4 are found at the ELF values that are smaller than 0.5. This means that electron localization in Fe_4 is greatly reduced due the Pauli repulsion exerted by the electron density concentrated in core regions. Silvi and Gatti[36] observed a similar behavior for the fcc lattice of Cu, where some attractors exhibit the ELF values of 0.38 and 0.20.

Attractors may be classified[21,22] according to properties of their basins. The concept of "synaptic order" is based on the number of core basins with which a valence basin shares common surfaces. Four valence monosynaptic attractors $V(Fe_{i=1,4})$ are found in Fe_4, which are displaced by 1.98 Å from the corresponding Fe nuclei. These attractors are related to regions where the valence electron density is highly delocalized and the ELF value is 0.279. Monosynaptic attractors[11] are usually associated with lone electron pairs or basins that emerge[37] during formation or cleavage of a chemical bond in sp compounds. For Fe_4, it is more appropriate to consider the $V(Fe_i)$ basins as regions where the nearest core basin $C(Fe_i)$ exerts the predominant influence on the distribution of electron density, in correspondence with the dominating $C(Fe_i) \Leftrightarrow V(Fe_i)$ covariance.[38] Llusar et al.[39] observed similar monosynaptic V(In) attractors located outside a K_8In_{11} cluster and noticed that the V(In) attractors are connected by pathways similar to those found in metals.

Disynaptic attractors $V_{i=1,2}(Fe_1,Fe_3)$, $V_{i=1,2}(Fe_1,Fe_4)$, $V_{i=1,2}(Fe_2,Fe_3)$, and $V_{i=1,2}(Fe_2,Fe_4)$ correspond to the basins which share common surfaces with two core basins $C(Fe_i)$. These attractors are located along the C_2 and C_2' symmetry axes at positions corresponding to the shorter edges of the distorted Fe_4 tetrahedron. For each edge, there are two pairs of attractors $V_1(Fe_{i=1,2},Fe_{j=3,4})$ and $V_2(Fe_{i=1,2},Fe_{j=3,4})$ placed at 1.424 Å at 1.971 Å from the corresponding nuclei, respectively. The $V_1(Fe_{i=1,2},Fe_{j=3,4})$ attractors, which are localized closer to the core basins, deliver a smaller ELF value of 0.438 due to a stronger Pauli repulsion than the attractors $V_2(Fe_{i=1,2},Fe_{j=3,4})$, where the ELF value is 0.490. Because the presence of two attractors along a line connecting two nuclei is rather unusual, it is instructive to consider the ELF topology between the $V_1(Fe_{i=1,2},Fe_{j=3,4})$ and $V_2(Fe_{i=1,2},Fe_{j=3,4})$ attractors in more detail. Our searching a critical saddle point of index 1 resulted in a point with the ELF value of 0.437, which is close to that of the $V_1(Fe_{i=1,2},Fe_{j=3,4})$ attractors. This means that both $V_1(Fe_{i=1,2},Fe_{j=3,4})$ and $V_2(Fe_{i=1,2},Fe_{j=3,4})$ basins form actually one extended valence basin $V_{1\cup2}(Fe_{i=1,2},Fe_{j=3,4})$ with the local maxima at the $V_2(Fe_{i=1,2},Fe_{j=3,4})$ positions. For simplicity, Figure 1 presents only the $V_1(Fe_{i=1,2},Fe_{j=3,4})$ attractors in order to visualize that these disynaptic basins correspond to four covalent two-center Fe−Fe bonds.

Four trisynaptic $V(Fe_1,Fe_2,Fe_3)$, $V(Fe_1,Fe_2,Fe_4)$, $V(Fe_2,Fe_3,Fe_4)$, and $V(Fe_1,Fe_3,Fe_4)$ attractors are found on the tops of triangular faces of the cluster, see Figure 1, at the distances of 1.803 Å from the corresponding Fe nuclei. The ELF value of 0.469 of these attractors is larger than that of $V_1(Fe_{i=1,2},Fe_{j=3,4})$ but smaller than that of $V_2(Fe_{i=1,2},Fe_{j=3,4})$. The presence of trisynaptic attractors reflects a trend for electron localization not only between the Fe−Fe pairs but also on the cluster faces. Thus, one may conclude that the Fe_4 cluster has four three-

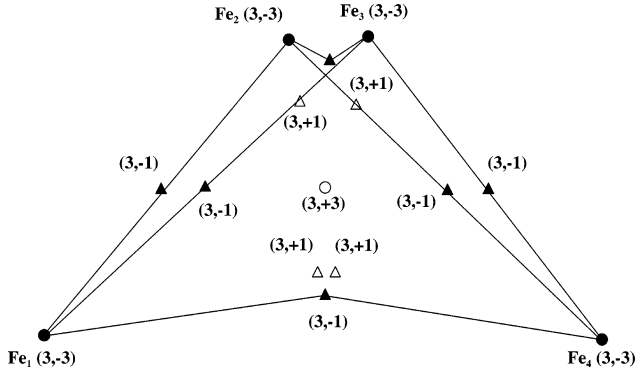

Figure 2. Electron density critical points of the order I = 0, 1, 2, and 3 in the Fe_4 cluster. Schematic lines joining attractors and bond critical points correspond to two-center bonds.

center covalent bonds. Feliz et al.[40] observed disynaptic $V_i(Mo_i,Mo_j)$ and trisynaptic $V(Mo_1,Mo_2,Mo_3)$ attractors in the Mo_3 subunit of the $[Mo_3S_4Cl_3(PH_3)_6]^+$ cluster. They found the value of ELF of 0.37 for the trisynaptic attractor.

There is a single tetrasynaptic attractor $V(Fe_1,Fe_2,Fe_3,Fe_4)$ in the center of the cluster which characterizes the electron density between four core basins $C(Fe_{i=1,4})$. This attractor is placed at the distance of 1.45 Å from each Fe nuclei. Its ELF value of 0.341 is larger than that of the monosynaptic $V(Fe_{i=1,4})$ attractor but smaller than the values of the $V_{i=1,2}(Fe_i,Fe_j)$ and $V(Fe_i,Fe_j,Fe_k)$ attractors. This tetrasynaptic $V(Fe_1,Fe_2,Fe_3,Fe_4)$ attractor may be interpreted as a four-center bond. Similar tetrasynaptic attractors may not be common in metal clusters because Wang et al.[41] did not find them in Sr_4, Yb_4, and Zn_4. On the other hand, Sun et al.[35] observed increased electron localization in the center of a distorted Al_6 octahedron corresponding to an ELF value of 0.5.

Another insight into the bonding properties of Fe_4 might be gained using Bader's concept[10] of atoms in molecules (AIM), where the molecular space is partitioned according to peculiarities of the one-electron density gradient field. The bonding interaction between a pair of atoms is indicated by the presence of a critical point $\mathbf{r}_c$ of index 1 that gives rise to a unique pair of trajectories of $\nabla(\rho(\mathbf{r}))$ originating at the critical point and terminating at two nuclei. According to Bader:[42] "the presence of a bond path provides a universal indicator of bonding between the atoms so connected".

All the critical points (CP) found in the gradient field of $\rho(\mathbf{r})$ are shown in Figure 2 where standard (r,s) designation is used; namely, the rank (r) of a CP refers to the number of nonzero eigenvalues and the signature (s) refers to the sum of signs of the Hessian eigenvalues. There are four local maxima corresponding to the Fe nuclei connected through six saddle critical points $(3,-1)$ which indicate that there are six chemical bonds in the cluster. These bonds may be schematically visualized as the edges of the distorted tetrahedron. Furthermore, there are four saddle critical points $(3,+1)$ and one local minimum $(3,+3)$ positioned at the center of the cluster. The minimum in the gradient field coincides with the local maximum of the ELF field that corresponds to the $V(Fe_1,Fe_2,Fe_3,Fe_4)$ attractor.

One should anticipate that the bonding in Fe_4 has a metallic type. The energetic criteria for such a bonding as suggested by Bianchi et al.[43] are: (1) the potential energy density $V(\mathbf{r}_c) < 0$ in the bond critical point (BCP) $\mathbf{r}_c$, (2) the kinetic energy density $G(\mathbf{r}_c) \cong |V(\mathbf{r}_c)|$, (3) the local electronic energy density $E(\mathbf{r}_c) < 0$ with $|E(\mathbf{r}_c)| \cong 0$. The value of the electron density $\rho(\mathbf{r}_c)$ obtained for the longer Fe_1-Fe_2 and Fe_3-Fe_4 bonds is 0.052 e/Bohr^3, which is smaller than the value of 0.076 e/Bohr^3 calculated for the shorter $Fe_{i=1,2}-Fe_3$ and $Fe_4-Fe_{i=1,2}$ bonds. For both types of bonds, the Laplacian $\nabla^2\rho(\mathbf{r}_c)$ is positive with the values of 0.055 and 0.014 e/Bohr,[5] respectively. The kinetic energy values are 0.030 and 0.061 Hartree/Bohr^3 while the potential energy density values are −0.048 and −0.087 Hartree/Bohr^3, respectively. This indicates a rather essential delocalization of the electron density around the BCPs. The metallic character of bonding is further confirmed by values of −0.018 and −0.026 Hartree/Bohr^3 of the local electronic energy density $E_e(\mathbf{r}_c)$ for the longer and shorter Fe−Fe bonds, respectively.

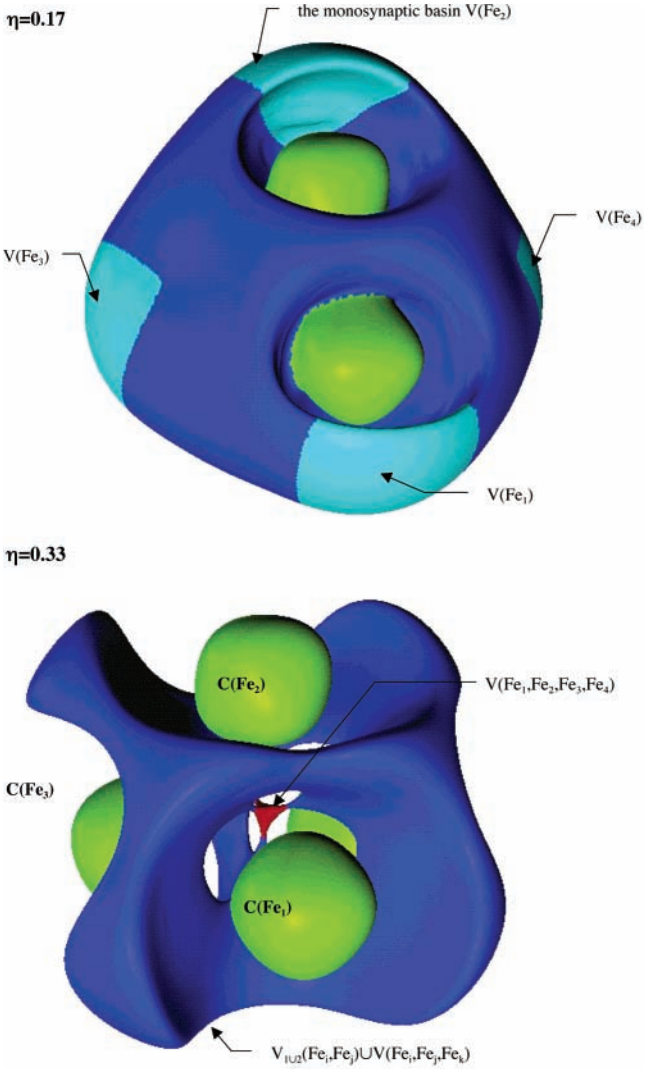

Figure 3. Three-dimensional representation of the Fe_4 ELF for $\eta(\mathbf{r}) = 0.17$ and 0.33. Disynaptic $V_{i=1\cup2}(Fe_i,Fe_j)$ and trisynaptic $V(Fe_i,Fe_j,Fe_k)$ valence basins are shown in blue as one super-basin.

The Fe_4 ELF is presented in Figure 3 for two η values of 0.17 and 0.33. The core basins $C(Fe_{i=1,4})$ are shown in green, the valence electron density regions are in violet, the monosynaptic basins $V(Fe_{i=1,4})$ are in blue, and the tetrasynaptic $V(Fe_1,Fe_2,Fe_3,Fe_4)$ basin is in red. For $\eta = 0.17$, there is a large domain whose boundary possesses holes around the core basins. These holes may be attributed to the participation of inner-shell electrons in the bonding as discussed by Kohout et al.[19] Namely, the maxima associated with the inner- and outer-core regions are separated by smaller ELF values. At larger ELF values, one can see the $V(Fe_1,Fe_2,Fe_3,Fe_4)$ basin and the delocalized valence electron density $V_{1\cup2}(Fe_{i=1,2},Fe_{j=3,4})\cup V(Fe_i,Fe_j,Fe_k)$ basins flowing between the core basins. The existence of such a delocalized electron density may be attributed to the exchange (Pauli) and

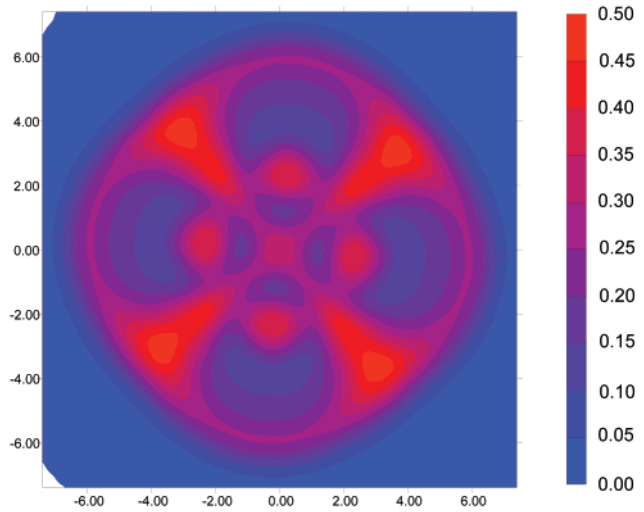

Figure 4. Two-dimensional plot of the Fe_4 ELF in an equatorial plane containing the V(Fe_1,Fe_2,Fe_3,Fe_4) attractor.

correlation effects that suppress random clustering of electrons.[44] An additional insight into the ELF topography may be gained from analyzing a two-dimensional cross section through an equatorial plane, which contains the V(Fe_1,Fe_2,Fe_3,Fe_4) attractor, as shown in Figure 4. As is seen, the core regions are surrounded by the holes with decreased electron localization. The Fe nuclei are surrounded by the electron density shells with the η values between 0.20 and 0.35. These shells are formed by the monosynaptic V(Fe_i) and outer disynaptic V_1($Fe_{i=1,2}$,$Fe_{j=3,4}$) basins.

The results of integration of the electron density over the localization basins are presented in Table 1. As is seen, the average population $\bar{N}$ of the C($Fe_{i=1,4}$) basins is 23.78 e and formally corresponds to the [Ar]$3d^6$ electron configurations of Fe_i. A small deviation from the exact value of 24 e can be explained by ambivalent character of electrons from 3d orbitals.[45] The mean value of the integrated spin density $\langle S_z \rangle$ is 1.47 e for the core basins, which corresponds to localization of three unpaired α-electrons. Two unpaired α-electrons are to be considered as distributed over four valence localization basins because the integrated spin density summed over each basin is 0.56 e, which yields two electrons for the whole cluster. Inspecting the $\langle S_z \rangle$ values in Table 1, one can see that the largest pile-up of the unpaired electron density has to be expected inside the $V_{1\cup2}$(Fe_i,Fe_j) basins. For the total basin population of 0.99 e, the integrated spin density equals 0.16 e. This result lends support to Goddard's interstitial-electron model,[46−48] according to which the valence electrons tend to localize into interstitial regions. A similar behavior was found[36] for the main valence basins in the fcc Al, Ca, Sc, and Cu metals. Note that the V_2(Fe_i,Fe_j) basins located closer to the C($Fe_{i=1,4}$) cores exhibit smaller values of $\langle S_z \rangle$. The electron density inside V_1(Fe_i,Fe_j) and V_2(Fe_i,Fe_j) is essentially delocalized and possesses the relative fluctuations (λ) of 0.87 and 0.91, respectively.

Figure 5 displays the α- and β-spin contributions to the ELF with $\eta = 0.30$ obtained according to the Kohout−Savin scheme,[49] which was recently applied[50] to studying different hydrocarbon radicals. From comparison of the contributions, one may conclude that the α-spin electron density is localized in the core regions while the β-spin electron density has a delocalized character along with pile-ups in the core regions. For larger ELF values, contributions of the α-spin electron density into the valence electron density are more noticeable.

Since the electron density is given as the sum of squared spin orbitals, it is interesting to consider partial contributions

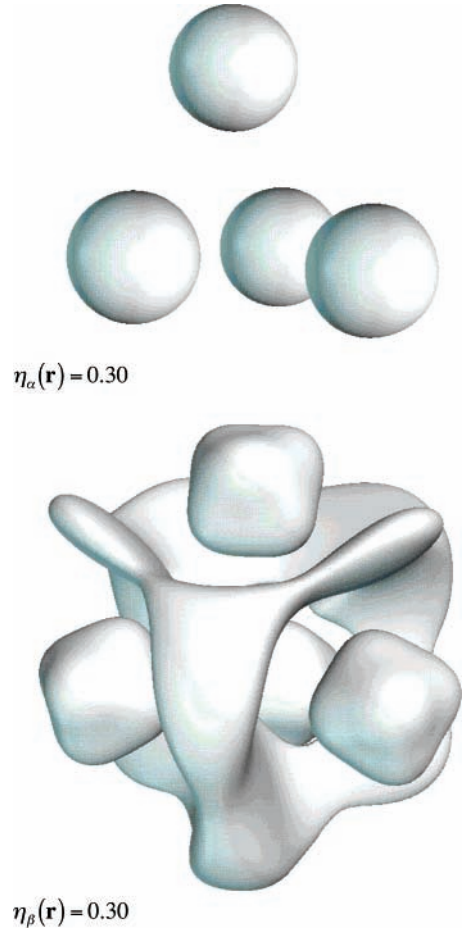

Figure 5. Isosurfaces of the ELF calculated using the α-spin orbitals for $\eta_\alpha(\mathbf{r}) = 0.30$ and the β-spin−orbitals for $\eta_\beta(\mathbf{r}) = 0.30$.

from different spin orbitals. Figure 6 presents contributions from the valence spin orbitals for the V_1(Fe_1,Fe_3) and V_2(Fe_1,Fe_3) basins. One may see that the largest contribution into V_1(Fe_1,Fe_3) comes from two α-spin orbitals: the highest occupied spin orbital (HOMO) and that next to the HOMO (HOMO-1). These two spin orbitals contribute approximately 0.1 e each, which is consistent with associating this basin with the Fe_1−Fe_3 bond. Contributions from the β-spin orbitals are much smaller and do not exceed 0.04 e. For the V_2(Fe_1,Fe_3) basin, contributions from the HOMO and HOMO-1 decrease to 0.01 e in accord with the characterization of the basin as a region close to the iron cores. A relatively large population (0.94 e) of the trisynaptic V(Fe_i,Fe_j,Fe_k) basin indicates that the electron density piles up near triangular faces of the cluster. However, this density is highly delocalized according to the values of 0.78 and 0.83 for the variance and relative fluctuation, respectively. Also, there is no essential concentration of α-electrons since the integrated spin density is 0.03 e. The largest contribution to V(Fe_1,Fe_2,Fe_3) comes from the 37th highly symmetric α- and β-spin orbitals composed of the $3d_{z^2}$ atomic orbitals, see Figure 7.

A similar behavior is observed for the V(Fe_1,Fe_2,Fe_3,Fe_4) tetrasynaptic basin where the largest contribution of 0.04 e comes from the 37th α- and β-spin orbitals as well. Among all other valence basins, this basin has the smallest population of 0.14 e, which may be attributed to its location inside of four core basins. The integrated spin density of this basin does not show any preference between α- or β-electrons. A large "Pauli pressure" exerted by the C(Fe_i) basins upon the V(Fe_1,Fe_2,Fe_3,Fe_4) basin is reflected by a large uncertainty in attributing the basin population because the relative fluctuation is 0.96.

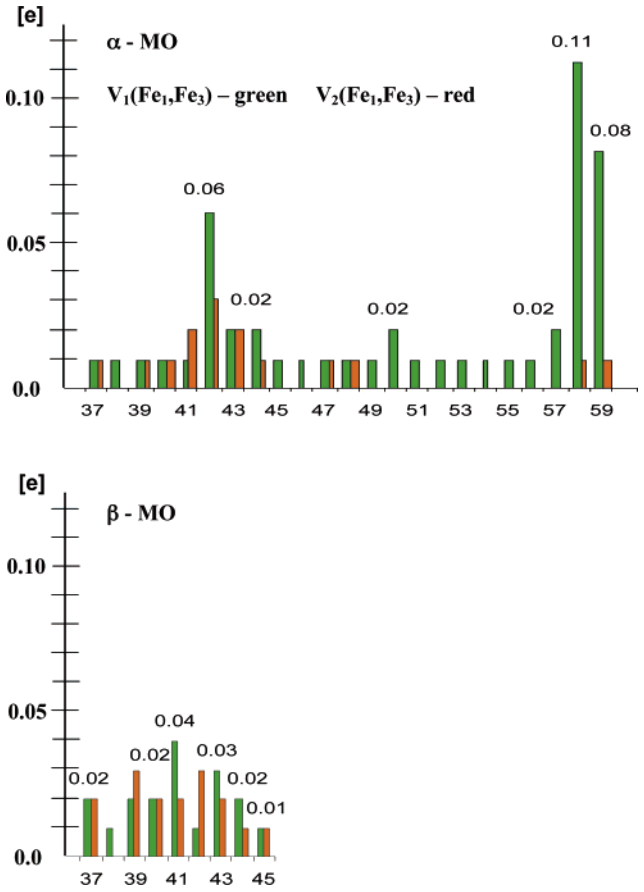

Figure 6. Contributions (≥ 0.01 e) from the α- and β-spin orbitals to the electron density inside two exemplary disynaptic basins $V_1(Fe_1,Fe_3)$ and $V_2(Fe_1,Fe_3)$.

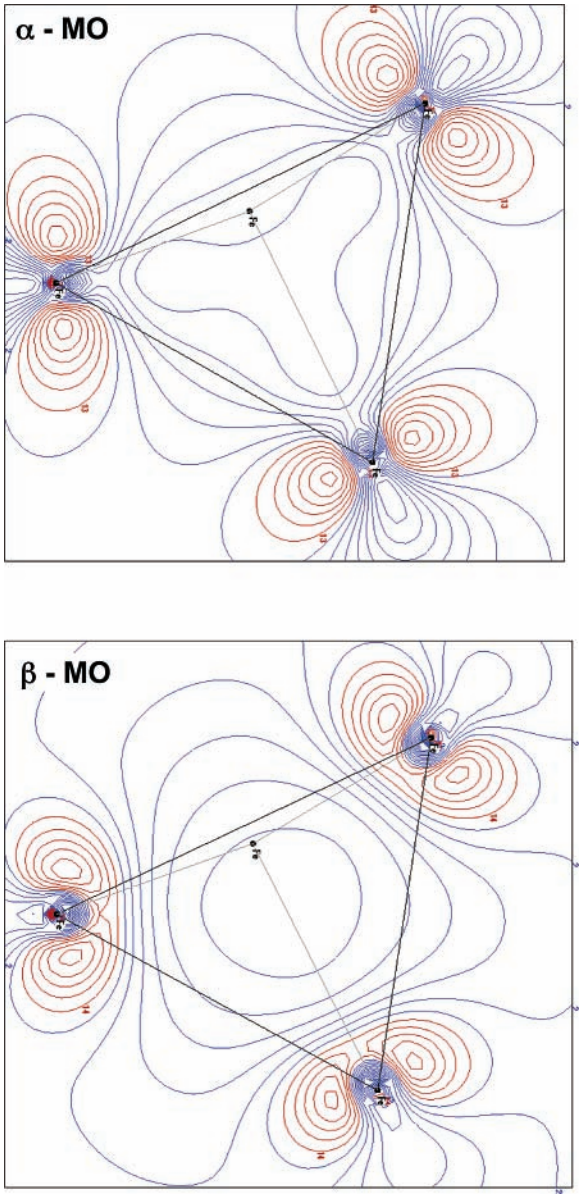

Figure 7. The 37th spin orbital, which yields the largest contribution to the electron density inside the trisynaptic $V(Fe_1,Fe_2,Fe_3)$ and tetrasynaptic $V(Fe_1,Fe_2,Fe_3,Fe_4)$ basins (top and bottom panels, respectively).

As previously emphasized,[51] the dominant feature of interactions between transition metal atoms M and M′ is reflected by the large values of the metal−metal covariance function cov(M,M′) found for the C(M) and C(M′) core basins and the AIM atomic basins covariance $\lambda_c(\rho)$. In the case of the Fe_4 cluster, the values of the $C(Fe_1)\leftrightarrow C(Fe_2)$ and $C(Fe_1)\leftrightarrow C(Fe_{i=3,4})$ covariances are 0.16 and 0.26, respectively. This means that the covariance is essentially larger for the shorter Fe−Fe bonds. Using the AIM partitioning, the $cov(Fe_i,Fe_j)$ values are 0.49 and 0.74 while the topological bond orders ($2*\lambda_c(\rho)$) are 0.98 and 1.48, respectively. One can surmise that delocalization of the electron density between the C(Fe) core basins appears to play an essential role in the metal−metal bonding.

5. Conclusions

The results of our topological analysis of the electron density in the ground-state iron tetramer allow several conclusions: (1) The electron localization in all valence regions of Fe_4 is smaller than 0.5, i.e., the value that corresponds to a homogeneous electron gas of the same density. Thus, the valence electrons are essentially delocalized in Fe_4. (2) Our topological analysis of the electron localization function revealed 21 local maxima corresponding to the mono-, di-, tri-, and quatrosynaptic attractors, which emphasizes a spatially delocalized character of the multicenter bonding in Fe_4. Our atom-in-molecule analysis of the electron density yielded six two-center Fe−Fe bonds corresponding to the classic Lewis description. (3) Localization of the valence electrons inside interstitial regions corresponds to ordinary two-center Fe−Fe bonds, while three-center Fe−Fe−Fe bonds originate from the electron density piled up near triangular faces of the slightly distorted tetrahedral nuclear frame. Some amount of the electron density piles up between four iron cores, which corresponds to a four-center Fe−Fe−Fe−Fe bond. (4) The area of the most delocalized electron density, found at the distance of ∼1.97 Å around the cluster, contains contributions from the monosynaptic $V(Fe_i)$ and outer-disynaptic $V_1(Fe_i,Fe_j)$ basins. (5) High delocalization of the electron density inside all the valence basins is reflected in rather large values of the relative fluctuation whose range is from 0.83 to 0.96. (6) From fourteen unpaired electrons of the ground-state Fe_4 cluster, twelve are localized at four core basin $C(Fe_{i=1,4})$ and two electrons are delocalized over the valence region.

Acknowledgment. S.B. thanks the "Wroclaw Centre for Networking and Supercomputing", where a part of the computations were performed, for the granted time. The Marie Curie Development Host Fellowship program supported the work of S.B., contract no. HPMD-CT-2000-00055. The authors are solely responsible for the information communicated and it does

not represent the opinion of The European Community. The European Community is not responsible for any use that might be made of data appearing therein. G.L.G. was partially supported from NASA Ames Research Center through contract NAS2-99092 to Eloret Corporation. This work was also supported in part by the Army High Performance Computing Research Center (AHPCRC) under the auspices of the Department of the Army, Army Research Laboratory (ARL) under Cooperative Agreement number DAAD19-01-2-0014. The content of which does not necessarily reflect the position or the policy of the government, and no official endorsement should be inferred. J.A. was supported by Universitat Jaume I-Fundacio Bancaixa, Project P1B99-02.

References and Notes

(1) Moskowits M.; DiLella, D. P. *J. Chem. Phys.* **1980**, *73*, 4917. Purdum, H.; Montano, P. A.; Shenoy, G. K.; Morrison, T. *Phys. Rev. B* **1982**, *25*, 4412. Rohlfing, E. A.; Cox, D. M.; Kaldor, A.; Johnson, K. H. *J. Chem. Phys*. **1984**, *81*, 3846. Cox, D. M.; Trevor, D. J.; Whetten, R. L.; Rohlfing, E. A.; Kaldor, A. *Phys. Rev. B* **1985**, *32*, 7290. Leopold, D. G.; Lineberger, W. C. *J. Chem. Phys*. **1986**, *85*, 51. Brucat, P. J.; Zheng, L.-S.; Pettiette, C. L.; Yang, S.; Smalley, R. E. *J. Chem. Phys*. **1986**, *84*, 3078. Nour, E. M.; Alfaro-Franco, C.; Gingerich, K. A.; Laane, J. *J. Chem. Phys.* **1987**, *86*, 4779. Loh, S. K.; Hales, D. A.; Lian, L.; Armentrout, P. B. *J. Chem. Phys*. **1989**, *90*, 5466. Parks, E. K.; Klots, T. D.; Riley, S. J. *J. Chem. Phys*. **1990**, *92*, 3813. Yang, S.; Knickelbein, M. B. *J. Chem. Phys*. **1990**, *93*, 1533. Lian, L.; Su, C.-X.; Armentrout, P. B. *J. Chem. Phys*. **1992**, *97*, 4072. Lian, L.; Su, C.-X.; Armentrout, P. B. *J. Chem. Phys*. **1992**, *97*, 4072. Billas, I. M. L.; Châtelain, A.; Heer, W. A. de *Science*, **1994**, *265*, 1682. Wang, L. S.; Cheng, H. S.; Fan, J. *J. Chem. Phys*. **1995**, *102*, 9480. Armentrout, P. B. In *Metal*−*Ligand Interactions: Structure and Reactivity*, Vol. 474 of NATO Advanced Studies Institute, Science Series C: Mathematical and Physical Sciences; Russo, N., Salahub, D. R., Eds.; Kluwer Academic Publishers: Amsterdam, 1996; p 23. Châtelain, A.; Heer, W. A. *Z. Phys. D* **1997**, *40*, 160. Haslett, T. L.; Bosnick, K. A.; Fedrigo, S.; Moskowits, M. *J. Chem. Phys.* **1999**, *111*, 6456. Châtelain, A *Philos. Mag.* B **1999**, *79*, 1367. Wang, L. S.; Li, X.; Zhang, H. F. *Chem. Phys*. **2000**, *262*, 53. Markin, E. M.; Sugawara, K. *J. Phys. Chem. A* **2000**, *104*, 1416. Armentrout, P. B. *Annu. Rev. Phys. Chem*. **2001**, *52*, 423−61.

(2) Morse, M. D. *Chem. Rev.* **1986**, *86*, 1049. Salahub, D. R. In *Ab initio Methods in Quantum Chemistry II*; Lawley, K. P., Ed.; Wiley: New York, 1987; pp 447−520. Dhar, S.; Kestner, N. R. *Phys. Rev. A* **1988**, *38*, 1111. Tomonari, M.; Tatewaki, H. *J. Chem. Phys*. **1988**, *88*, 1828. Pavão, A. C.; Taft, C. A.; Hammond, B. L.; Lester, W. A., Jr. *Phys. Rev. B* **1989**, *40*, 2879. Noro, T.; Ballard, C.; Palmer, M. H.; Tatewaki, H. *J. Chem. Phys*. **1994**, *100*, 452. Yanasigava, S.; Tsuneda, T.; Hirao, K. *J. Chem. Phys*. **2000**, *112*, 545. Barden, C. J.; Rienstra-Kiracofe, J. C.; Schaefer, H. F., III *J. Chem. Phys*. **2000**, *113*, 690.

(3) Tatewaki, H.; Tomonari, M.; Nakamura, T. *J. Chem. Phys*. **1988**, *88*, 6419. Dunlap, B. I. *Phys. Rev. A* **1990**, *41*, 5691. Chen, J. L.; Wang, C. S.; Jackson, K. A.; Pederson, M. R. *Phys. Rev. B* **1991**, *44*, 6558. Cheng, H.-P.; Ellis, D. E. *J. Chem. Phys*. **1991**, *94*, 3735. Christensen, O. B.; Cohen, M. L. *Phys. Rev. B* **1993**, *47*, 13643. Gong, X. G.; Zheng, Q. Q. *J. Phys.: Condens. Matter* **1995**, *7*, 2421. Ballone, P.; Jones, R. O. *Chem. Phys. Lett.* **1995**, *233*, 632. Oda, T.; Pasquarello, A.; Car, R. *Phys. Rev. Lett*. **1998**, *80*, 3622. Andriotis, A. N.; Menon, M. *Phys. Rev. B* **1998**, *57*, 10069. Castro, M.; Jamorski, K.; Salahub, D. R. *Chem. Phys. Lett.* **1997**, *271*, 133. Diéguez, O.; Alemany, M. M. G.; Rey, C.; Ordejón, P.; Gallego, L. J. *Phys. Rev. B* **2001**, *63*, 205407. Bobadova-Parvanova, P.; Jackson, K. A.; Srinivas, S.; Horoi, M.; Köhler, C.; Seifert, G. *J. Chem. Phys.* **2002**, *116*, 3576. Duan, H. M.; Zheng, Q. Q. *Phys. Lett*. A **2001**, *280*, 333.

(4) Castro, M.; Salahub, D. R. *Phys. Rev. B* **1994**, *49*, 11842. Castro, M. *Int. J. Quantum Chem*. **1997**, *64*, 223. Gutsev, G. L.; Khanna, S. N.; Jena, P. *Phys. Rev. B* **2000**, *62*, 1604. Gutsev, G. L. *Phys. Rev. B* **2002**, *65*, 132417. Chrétien, S.; Salahub, D. R. *Phys. Rev. B* **2002**, *66*, 155425.

(5) Gutsev, G. L.; Bauschlicher, C. W., Jr. *J. Phys. Chem.* A **2003**, *107*, 7013.

(6) Reed, A. E.; Weinstock, R. B.; Weinhold, F. *J. Chem. Phys*. **1985**, *83*, 735. Reed, A. E.; Curtiss, L. A.; Weinhold, F. *Chem. Rev.* **1988**, *88*, 899.

(7) Michelini, M. C.; Sicilia, E.; Russo, N.; Alikhani, M. E.; Silvi, B. *J. Phys. Chem.* A **2003**, *107*, 4862.

(8) Gutsev, G. L.; Rao, B. K.; Jena, P.; Khanna, S. N. *J. Chem. Phys*. **2001**, *114*, 10738. Gutsev, G. L.; Bauschlicher, C. W., Jr. *J. Phys. Chem.* A **2003**, *107*, 4755.

(9) Becke, A. D.; Edgecombe, K. E. *J. Chem. Phys*. **1990**, *92*, 5387.

(10) Bader, R. F. W. *Atoms in Molecules: A Quantum Theory*, Oxford University Press: Oxford, 1994. Bader, R. F. W.; Essén H. *J. Chem. Phys*. 1984, *80*, 1943. Bader, R. F. W.; MacDougall, P. J.; Lau, C. D. H. *J. Am. Chem. Soc*. **1984**, *106*, 1594.

(11) Silvi, B.; Savin, A. *Nature* **1994**, *371*, 683.

(12) Häussermann, U.; Wengert, S.; Nesper, R.; *Angew. Chem., Int. Ed. Engl*. **1994**, *33*, 2073.

(13) Lewis, G. N. *J. Am. Chem. Soc*. **1916**, *38*, 762.

(14) Lewis, G. N. *Valence and the Structure of Atoms and Molecules*; Dover: New York, 1966.

(15) Savin, A.; Becke, A. D.; Flad, J.; Nesper, R.; Preuss, H.; von Schnering, H. G. *Angew. Chem., Int. Ed. Engl*. **1991**, *30*, 409.

(16) Dobson, J. F. *J. Chem. Phys*. **1991**, *94*, 4328.

(17) Dobson, J. F. *J. Chem. Phys*. **1993**, *98*, 8870.

(18) Burdett, K. J.; McCormick, T. A. *J. Phys. Chem. A* **1998**, *102*, 6366.

(19) Kohout, M.; Wagner, R. F.; Grin, Y. *Theor. Chem. Acc*. **2002**, *108*, 150.

(20) Silvi, B. *J. Phys. Chem. A* **2003**, *107*, 3081.

(21) Savin, A.; Silvi, B.; Colonna, F. *Can. J. Chem*. **1996**, *74*, 1088.

(22) Silvi, B. *J. Mol. Struct*. **2002**, *614*, 3.

(23) Bader, R. F. W.; Stephens, M. E.; *Chem. Phys. Lett.* **1974**, *26*, 445.

(24) Kohn, W.; Sham, L. J. *Phys. Rev. A* **1965**, *140*, 1133.

(25) Frisch, M. J.; Trucks, G. W.; Schlegel, H. B.; Scuseria, G. E.; Robb, M. A.; Cheeseman, J. R.; Zakrzewski, V. G.; Montgomery, J. A.; Jr.; Stratmann, R. E.; Burant, J. C.; Dapprich, S.; Millam, J. M.; Daniels, A. D.; Kudin, K. N.; Strain, M. C.; Farkas, O.; Tomasi, J.; Barone, V.; Cossi, M.; Cammi, R.; Mennucci, B.; Pomelli, C.; Adamo, C.; Clifford, S.; Ochterski, J.; Petersson, G. A.; Ayala, P. Y.; Cui, Q.; Morokuma, K.; Malick, D. K.; Rabuck, A. D.; Raghavachari, K.; Foresman, J. B.; Cioslowski, J.; Ortiz, J. V.; Baboul, A. G.; Stefanov, B. B.; Liu, G.; Liashenko, A.; Piskorz, P.; Komaromi, I.; Gomperts, R.; Martin, R. L.; Fox, D. J.; Keith, T.; Al-Laham, M. A.; Peng, C. Y.; Nanayakkara, A.; Gonzalez, C.; Challacombe, M.; Gill, P. M. W.; Johnson, B.; Chen, W.; Wong, M. W.; Andres, J. L.; Gonzalez, C.; Head-Gordon, M.; Replogle, E. S.; Pople, J. A. *Gaussian 98*, revision A.11, Gaussian, Inc.: Pittsburgh, PA, 1998.

(26) Wachters, A. J. H. *J. Chem. Phys.* **1970**, *52*, 1033.

(27) Hay, P. J. *J. Chem. Phys.* **1977**, *66*, 4377.

(28) Raghavachari, K.; Trucks, G. W. *J. Chem. Phys.* **1989**, *91*, 1062.

(29) Becke, A. D. *Phys. Rev. A* **1988**, *38*, 3098.

(30) Perdew, J. P.; Wang, Y. *Phys. Rev. B* **1992**, *45*, 13244.

(31) Noury, S.; Krokidis, X.; Fuster, F.; Silvi, B. *TopMod*; Paris **1997**.

(32) Noury, S.; Krokidis, X.; Fuster, F.; Silvi, B. *Comp. Chem*. **1999**, *23*, 597.

(33) Pepke, E.; Murray, J.; Lyons, J.; Hwu, T.-Z. SciaAn: Supercomputer Computations Research Institute: Florida State University, Tallahassee, FL, 1993.

(34) AIMPAC, McMaster University, Hamilton, Ont., Canada. Biegler-König, F. W.; Bader, R. F. W.; Tang, T.-H. *J. Comput. Chem*. **1982**, *3*, 317.

(35) Sun, Q.; Wang, Q.; Yu, Z.; Kumar, V.; Kawazoe, Y. *Phys. Rev. B* **2001**, *63*, 193408.

(36) Silvi, B.; Gatti, C. *J. Phys. Chem. A* **2000**, *104*, 947.

(37) Krokidis, X.; Noury, S.; Silvi, B. *J. Phys. Chem. A* **1997**, *101*, 7277.

(38) A covariance between the V(Fe_1) monosynaptic valence and core C(Fe_1) basins is 0.1 while the covariances calculated with the other basins do not exceed 0.02.

(39) Llusar, R.; Beltrán, A.; Andrés, J.; Silvi, B.; Savin, A. *J. Phys. Chem.* **1995**, *99*, 12483.

(40) Feliz, M.; Llusar, R.; Andrés, J.; Berski, S.; Silvi, B. *New J. Chem*. **2002**, *26*, 844.

(41) Wang, Y.; Flad, H.-J.; Dolg, M. *J. Phys. Chem. A* **2000**, *104*, 5558.

(42) Bader, R. F. W. *J. Phys. Chem. A* **1998**, *102*, 7314.

(43) Bianchi, R.; Gervasio, G.; Marabello, D. *Inorg. Chem*. **2000**, *39*, 2360.

(44) Kurth, S., Perdew, J. P. *Int. J. Quantum Chem*. **2000**, *77*, 814.

(45) Kohout, M., Savin, A. *J. Comput. Chem*. **1997**, *18*, 1431.

(46) McAdon, M. H.; Goddard, W. A., III. *Phys. Rev. Lett* **1985**, *55*, 2563.

(47) Li, M.; Goddard, W. A., III. *Phys. Rev. B* **1989**, *40*, 12156.

(48) McAdon, M. H.; Goddard, W. A., III. *J. Phys. Chem.* **1987**, *91*, 2607.

(49) Kohout, M.; Savin, A. *Int. J. Quantum Chem*. **1996**, *60*, 815.

(50) Melin, J.; Fuentalba, P. *Int. J. Quantum Chem*. **2003**, *92*, 382.

(51) Llusar, R.; Beltrán, A.; Andrés, J.; Fuster, F.; Silvi, B. *J. Phys. Chem. A* **2001**, *105*, 9460.